Journal of Power Sources 563 (2023) 232810

Contents lists available at ScienceDirect

Journal of Power Sources

journal homepage: www.elsevier.com/locate/jpowsour

Ultra-thin thermally grown silicon dioxide nanomembrane for waterproof perovskite solar cells

Myeongki Cho [a], Gyeong G. Jeon [c,e], Mingyu Sang [a], Tae Soo Kim [a], Jungmin Suh [a], So Jeong Shin [e], Min Jun Choi [e], Hyun Woo Kim [a], Kyubeen Kim [a], Ju Young Lee [a], Jeong Yeon Noh [a], Jong H. Kim [e], Jincheol Kim [c,d,**], Nochang Park [c,***], Ki Jun Yu [a,b,*]

[a] School of Electrical and Electronic Engineering, Yonsei University, Seoul, Republic of Korea
[b] Yonsei-KIST Convergence Research Institute, Yonsei University, Seoul, Republic of Korea
[c] New & Renewable Energy Research Center, Korea Electronics Technology Institute, Seong-Nam, Republic of Korea
[d] School of Engineering, Macquarie University Sustainable Energy Research Centre, Macquarie University, Sydney, Australia
[e] Department of Molecular Science and Technology, Ajou University, Suwon, Republic of Korea

HIGHLIGHTS

- Demonstrated room temperature thin film encapsulation using thermally grown SiO_2.
- Demonstrated encapsulation of perovskite solar cells without thermal decomposition.
- The thermally grown silicon dioxide nanomembrane is superior moisture barrier.
- The encapsulated perovskite solar cell was stable for 31 days underwater.

ARTICLE INFO

Keywords:
Perovskite solar cells
Room temperature encapsulation
Thin-film encapsulation
Water barrier
Long-term stability

ABSTRACT

Recently, perovskite solar cells (PSCs) have been attracting attention as the most promising alternative to conventional photovoltaics, mainly due to their high power conversion efficiency (PCE) of 25.7%. However, prior to commercialization, problems with their long-term stability caused by moisture should be solved. Accordingly, encapsulation is a crucial strategy for enhancing the long-term stability of PSCs, meaning a well-established strategy that includes an excellent barrier that protects them from the external environment while minimizing any damage during encapsulation is required. In this study, a room temperature thin-film encapsulation (RT-TFE) strategy is applied by transferring a defect-free thermally grown silicon dioxide nanomembrane (t-SiO_2 NM), which is a well-known superior water molecule barrier, onto the PSCs. The average PCE of the devices decreased by only 0.012% with a standard deviation of 0.4249 during the entire encapsulation process, which was achieved by minimizing any thermal degradation of the photovoltaic components, including the perovskite and hole transport layers. This t-SiO_2 NM successfully protected the PSC from external water molecules in an underwater condition for 31 days at room temperature, which is the longest reported survival time of encapsulated PSCs. As a result, the RT-TFE PSC maintained more than 98% of the initial efficiency.

1. Introduction

Organic-inorganic lead halide perovskite is known as an exceptional light absorption material for photovoltaic devices due to its excellent photoelectronic properties, including a high light absorption coefficient, high carrier mobility, long carrier diffusion lengths, low exciton binding energy, and adjustable bandgap [1–5]. In addition to these excellent optoelectronic properties, lightweight and flexible perovskite solar cells (PSCs) can be fabricated on flexible thin films with low manufacturing costs due to the possibility of solution processing, offering an attractive

* Corresponding author.
** Corresponding author.
*** Corresponding author.
E-mail addresses: jincheol.kim@mq.edu.au (J. Kim), ncpark@keti.re.kr (N. Park), kijunyu@yonsei.ac.kr (K.J. Yu).

https://doi.org/10.1016/j.jpowsour.2023.232810
Received 11 September 2022; Received in revised form 7 February 2023; Accepted 10 February 2023
Available online 17 February 2023

commercial advantage as next-generation photovoltaics [6–11]. Since the first PSC was reported in 2009, their power conversion efficiency (PCE) has rapidly increased from 3.8% to 25.7%, and photovoltaics based on perovskite are currently in the spotlight as a promising alternative to silicon-based solar cells [12,13]. However, despite their high PCE, flexibility, and low manufacturing costs, the most challenging issue facing PSCs is long-term stability, which must be resolved before they can be commercially practical in outdoor environments [14–16]. The major factor that impedes the lifetime of PSCs is instability caused by moisture from external environments [17,18]. Due to the high reactivity between the organic-inorganic halide perovskite materials and water molecules, the photoactive perovskite layer is irreversibly decomposed by moisture, directly resulting in permanent performance degradation of the photovoltaics [19,20]. To prevent this performance degradation caused by moisture, numerous extrinsic encapsulation strategies for completely protecting PSCs from water molecules in external environments have been studied, usually by placing a physical barrier on the outermost layer of the PSCs [21–30].

Encapsulation not only directly protects the device from external moisture, but also blocks the leakage of toxic heavy metals and traps the volatile gas to restrict endogenous decomposition of the perovskite [22,31,32]. The encapsulation layer of PSCs should have low water and oxygen molecule transmittance, high dielectric constant and transparency, thermal stability, chemical inertness, and mechanical robustness [33]. In particular, the water vapor transmission rate (WVTR), which is the main performance indicator of the encapsulation barrier, should be within the range of 1×10^{-3} to 1×10^{-6} g m^{-2} day^{-1} to effectively prevent moisture ingress [34]. Furthermore, during the entire encapsulation process of PSCs, their intrinsic performance must be protected from external interventions such as unwanted UV, incidental heat, and high-energy plasma ions [29,35–37].

Traditionally, glass has been used as an encapsulation material in the glass-to-glass cover encapsulation method due to its superior water barrier property ($WVTR_{glass} < 1 \times 10^{-6}$ g m^{-2} day^{-1}). Here, hot-melting film, UV or heat-curable epoxy, and glass-frit are used as the adhesive materials [38]. However, cover encapsulation is inherently bulky and heavy, rendering it unsuitable for flexible PSCs. Furthermore, when the photovoltaics and barrier cover are bonded, external energy, such as UV or heat, must be injected to cure the adhesive materials, which can degrade the PSCs [23–26,34,39,40]. Fu et al. encapsulated PSCs using three hot-melting films (polyurethane, polyolefin, and ethylene vinyl acetate) with glass sheets [41]. However, during the encapsulation process, when the laminating temperature of the hot-melting sheet reached 90 °C, performance degradation of the PSCs was induced through changes in the interface of the solar cell. Moreover, at temperatures higher than 100 °C, deterioration of the devices occurred due to the decomposition of the perovskite layer. Similarly, during the process of hot press sealing for cover encapsulation using polyisobutylene, a decrease in the performance of devices occurred [23]. Matteocci et al. reported that UV irradiation used for epoxy curing during encapsulation reduced the PCE of PSCs [24]. When TiO_2-based PSCs are exposed to UV, degradation of the photovoltaics is caused by trap-assisted recombination at the TiO_2 interface. Martins et al. demonstrated low temperature laser-assisted glass frit encapsulation [27]. Despite the short-term and local laser irradiation, local heat during the sintering of the glass frits induced thermal degradation in the hole transport materials (HTMs).

Generally, thin film encapsulation (TFE) is used for organic optoelectronic devices such as organic light-emitting diodes and organic photovoltaics that must be protected from moisture and oxygen [42–46]. In contrast to glass-to-glass encapsulation using rigid glass sheets, TFE consisting of single or multi-stacked nanomembranes using chemical vapor deposition (CVD) or atomic layer deposition (ALD) can be applied to flexible devices due to its mechanical flexibility [45,47]. Accordingly, TFE provides a promising strategy for enhancing the long-term stability of flexible PSCs based on solution processes on flexible substrates [22,29,44,48,49]. However, since the TFE layer has a higher WVTR than a thick and rigid glass sheet, it is relatively difficult to achieve reasonable high long-term stability of the solar cells against external moisture. In the early stage of TFE development, single or multiple layers composed of inorganic nanomembranes, such as SiO_x, SiN_x, Al_2O_3, HfO_2, ZrO_2, and TiO_2, were deposited on PSCs using CVD or ALD [50,51]. However, preparing nanomembranes deposited by CVD and ALD that are free from defects creating pathways for external molecules, such as voids, pinholes, and particles, is very difficult [52]. Furthermore, to minimize the defects in the encapsulation layer, TFE requires either a high temperature in vacuum deposition processes [21,22] or high-energy ions in plasma-enhanced deposition processes, which can also result in the degradation of PSCs [29]. Accordingly, the high temperature processes of inorganic TFE are unsuitable for encapsulating PSCs. To encapsulate PSCs more effectively, hybrid TFEs with alternating organic and inorganic layers have been studied [22,29]. In a hybrid TFE, multiple inorganic layers robustly prevent water and oxygen transmission, while the organic layers cover defects in the interface of the inorganic layers [53]. Therefore, hybrid TFEs can provide a longer penetration path and better encapsulation performance than single-component TFEs, even with relatively low temperature manufacturing processes [54,55]. Lee et al. demonstrated a hybrid TFE that was achieved by stacking poly-1,3,5-trimethy-1,3,5-trivinyl cyclotrisiloxane and Al_2O_3 deposited layer-by-layer using initiated chemical deposition and ALD at a relatively low temperature (<60 °C) [22]. The encapsulated PSC maintained 97% of its initial PCE after 300 h at 50 °C and 50% relative humidity (RH). Wang et al. proposed a multi-layer TFE strategy utilizing an alucone layer to protect PSCs from oxidant precursors and oxygen plasma during plasma-enhanced ALD [29]. The PSCs were encapsulated with multi-layers of alucone and Al_2O_3 deposited at 50 °C, causing minimal degradation of the photovoltaic cells due to heat. At 30 °C and 80% RH, the encapsulated PSC retained 96% of its original PCE after 2000 h. However, with all these various low temperature TFE strategies for preventing the thermal degradation of PSCs, the performance of the PSCs decreased during the encapsulation process. Furthermore, degradation of the PSCs inevitably accelerated as the deposition temperature was increased further to achieve high barrier performance [22,29,56]. Thus, a novel TFE strategy based on a low temperature encapsulation process that ensures the high performance of PSCs without any degradation is highly desirable.

Herein, we demonstrate a novel room temperature thin-film encapsulation (RT-TFE) strategy to enhance the long-term stability of PSCs. This is achieved by encapsulating the PSCs with a thermally grown silicon dioxide nanomembrane (t-SiO_2 NM) (<500 nm) grown at 1100 °C, which could not be applied in the fabrication of the conventional PSCs. Silicon dioxide grown at a high temperature (>800 °C) on a single crystalline silicon surface by thermal oxidation is a defect-free material that is well known as a superior barrier to water molecules [52,57,58]. In this work, we transferred t-SiO_2 NM with its previously-mentioned superior barrier performance to PSCs at room temperature while minimizing any thermal degradation of the photovoltaics. The average PCE value of the 17 employed devices, which were typical thermally unstable $MAPbI_3$/2,2′,7,7′-tetrakis (N,N-dip-methoxyphenylamine)-9,9′-spirobifluorene (Spiro-OMeTAD) based n-i-p type PSCs, only changed by 0.012% after the entire RT-TFE process. We evaluated the performance of the t-SiO_2 encapsulation layer using an electrical calcium test. The t-SiO_2 NM was an excellent water molecule barrier, recording a water transmission rate (WTR) of 1.53×10^{-3} g m^{-2} day^{-1} when directly exposed to DI water at 85 °C. Moreover, the t-SiO_2 encapsulation layer prevented liquid-state water molecules from penetrating the PSC for 31 days at room temperature and the device maintained more than 98% of its initial PCE. Our RT-TFE approach effectively improved the long-term stability of PSCs based on $MAPbI_3$/spiro-OMeTAD, which is particularly sensitive to heat and moisture, and successfully encapsulated the devices without causing any damage.

2. Result and discussion

2.1. Room temperature thin-film encapsulation process

Thin-film encapsulation by applying an extrinsic moisture barrier to the outermost layer of PSCs is an outstanding strategy for enhancing their long-term stability. In a typical solution-based process for thin-film PSC fabrication, an annealing process is needed to form each component, as well as organic-inorganic hybrid perovskite and organic HTM crystallization [59,60]. However, PSC components, especially HTMs, are susceptible to stress from unwanted external heat during TFE processes [61,62]. Thus, careful application of annealing during the encapsulation processing of the fabricated PSCs was required. Accordingly, we adopted the RT-TFE strategy to enhance the long-term stability of the PSCs while minimizing any damage to the devices.

Fig. 1a shows an exploded schematic diagram of the RT-TFE PSC. The encapsulation barrier for protecting the perovskite solar cells from external moisture comprises three layers. The top layer is a t-SiO_2 encapsulation layer, which protects the device from extrinsic instability. The thin intermedium layer is a SU-8 buffer layer (~4 GPa) to prevent any mismatch in Young's modulus between the top layer (~57 GPa) and the bottom layer (~1.5 MPa). The bottom layer is a Kwik-Sil adhesive layer, to form bonds between the PSC and silicon dioxide, SU-8 bilayer. The detailed device layer configuration of the RT-TFE PSC is presented in a schematic diagram of the structure in Fig. 1b. The cross-sectional scanning electron microscopy (SEM) images of the device's top layers identify the outermost 500 nm t-SiO_2 layer. Fig. 1c displays an illustration of the six main steps of the RT-TFE process, the details of which appear in the experimental section. i) The process starts with pre-polishing a handling silicon wafer to a thickness of 100 μm. ii) The pre-polished wafer is then subjected to thermal oxidation at ~1100 °C to grow silicon dioxide (500 nm) for the moisture barrier. iii) Sequentially, a solution-processed UV curable epoxy is deposited through surface treatment and is then spin-coated and cured. iv) The silicone adhesive is applied to the buffer layer. v) Next, the encapsulation layer stacked on the handling wafer is bonded to the desired target PSC in a glove box in a

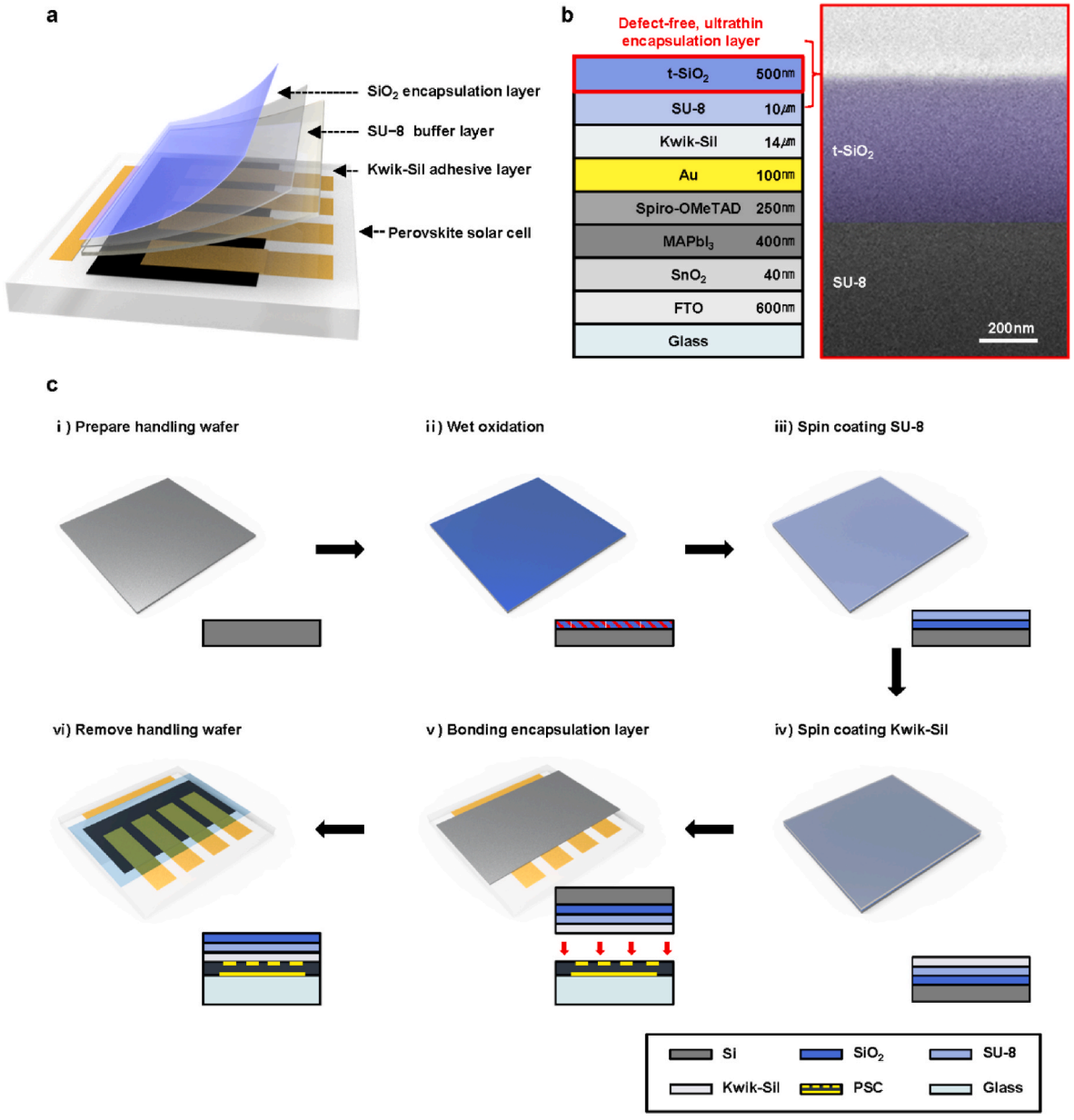

Fig. 1. RT-TFE strategy for PSCs: a) exploded-view schematic of the key functional layers of the RT-TFE PSC; b) (left) illustration of the entire RT-TFE PSC structure, (right) cross-sectional SEM image of the defect-free, ultrathin 500 nm t-SiO_2 NM encapsulation layer; c) fabrication process of the RT-TFE with t-SiO_2 NM on a PSC.

nitrogen environment. vi) Finally, the handling silicon wafer is etched using an XeF_2 etcher. The XeF_2 etcher is a tool that is mainly used in the field of micro electron mechanical systems manufacturing, where it is used to perform isotropic dry etching of Si at room temperature in a pure chemical process with high selectivity [63].

2.2. Application of RT-TFE to PSCs

Spiro-OMeTAD is commonly used as an HTM for high-efficiency and intrinsically stable PSCs, because of its appropriate electrical properties [64,65]. Although spiro-OMeTAD is relatively stable at room temperature compared to other HTM materials, the thermal stability is very poor due to a low glass transition temperature (T_g) of approximately 125 °C [60,66]. Moreover, dopants of spiro-OMeTAD, such as Bis(trifluoromethylsulfonyl)imide lithium salt (Li-TFSI) and 4-tert-Butylpyridine (t-BP), further lower the T_g and enhance the hygroscopicity of spiro-OMeTAD [67–70]. To avoid the previously mentioned degradation of perovskite solar cells, we demonstrated the RT-TFE strategy to minimize thermal and moisture degradation during the encapsulation process. Then, the properties of the encapsulated PSC through the RT-TFE process were evaluated.

Fig. 2a shows the current density-voltage (J-V) curves of an encapsulated solar cell. Each parameter was measured before and after encapsulation of the device. The pristine cell had a V_{oc} value of 1.07 V, a J_{sc} value of 21.95 mA cm^{-2}, and a fill factor (FF) of 80.10%, while the RT-TFE cell had a V_{oc} value of 1.05 V, a J_{sc} value of 22.40 mA cm^{-2}, and a FF value of 79.39%, yielding PCEs of 18.87% and 18.76%, respectively. We noted that the PCE drop ratio after encapsulation was only 0.11%. As shown in Fig. 2b, the PSC had a similar external quantum efficiency (EQE) before and after encapsulation within the solar spectrum. The integrated J_{sc} values over the AM 1.5G solar spectrum were also calculated. The integrated $J_{eqe,sc}$ over AM 1.5G solar spectrum for both cells were comparable, at 21.22 and 21.29 mA cm^{-2} before and after encapsulation, due to preservation of the spiro-OMeTAD layer during the RT-TFE process. Reactive ion etchers generate incidental heat due to the physicochemical etching methods conventionally used in silicon etching processes. In contrast, our encapsulation strategy using the XeF_2 etcher, which is a pure chemical etching method at room temperature, successfully prevented the deterioration of HTM and resulted in minimal degradation of the PSCs (Fig. S1). In Fig. 2c, the 17 PSCs fabricated using the RT-TFE strategy exhibited distinguished reproducibility according to the statistical distribution, with only a 0.012% average efficiency loss and a standard deviation of 0.4249. The encapsulated samples did not exhibit any visual changes compared to the pristine sample, as displayed in Fig. 2d.

2.3. Electrical calcium test to evaluate the performance of tg-SiO2 encapsulation layer

To evaluate the water barrier performance of t-SiO_2, the WTR was studied by applying t-SiO_2 with a thickness of 500 nm on the 100 nm calcium samples. The same thicknesses of parylene C, sputter-deposited SiO_2, PEVCD-deposited SiO_2, and three layers of 50 nm/127 nm Al_2O_3/parylene C pair encapsulation layers were also studied as the control group. Here, 1 cm^2 of calcium samples were encapsulated with a water barrier having an area of 2.25 cm^2 in the same manner as the RT-TFE. A

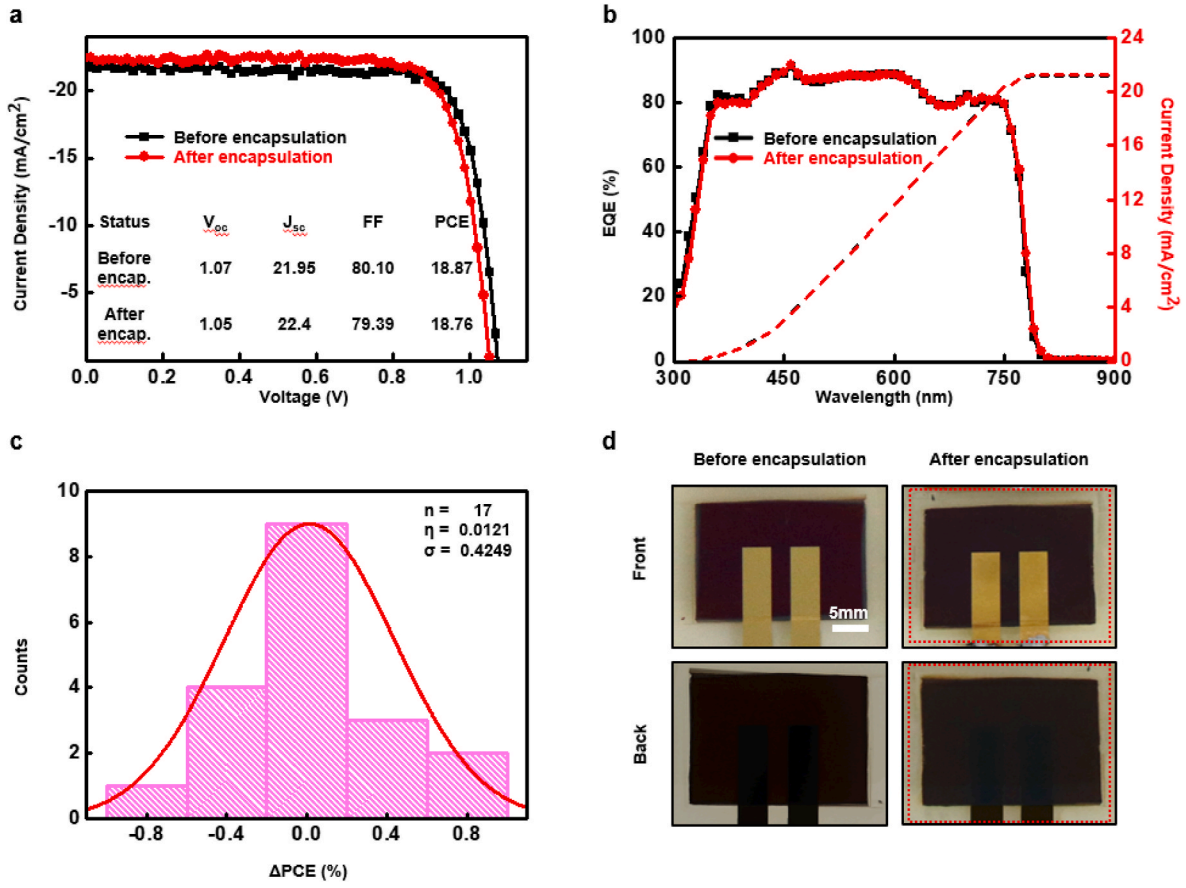

Fig. 2. Characteristics of PSC before and after RT-TFE: a) J-V curves of the PSC before and after encapsulation; b) EQE spectra and integrated current density of the PSC before and after encapsulation; c) histograms of the efficiency change distribution of 17 samples of PSCs after RT-TFE, fitted with Gaussian distributions (red line); d) photograph of front-side (top) and back-side (bottom) PSC, before (left) and after (right) encapsulation. The encapsulated area is 3.74 cm^2 in the red box. (For interpretation of the references to colour in this figure legend, the reader is referred to the Web version of this article.)

resin mold with a window of 1 cm^2 on the bottom was then fixed to the encapsulated calcium samples using a UV-curable epoxy. Subsequently, the resin mold was filled with DI water and the silicone lid was covered to minimize water evaporation.

Fig. 3a displays optical microscope images of calcium samples encapsulated with t-SiO_2 and other reference layers before and after exposure to DI water at room temperature. Although the calcium in all the control samples was oxidized in a pin-hole manner after a few minutes from reacting with water molecules that had passed through the encapsulation layer, the t-SiO_2 encapsulated calcium sample maintained its initial state. In Fig. 3b, the normalized resistances of all the samples were measured during a water permeation test at room temperature. In humid condition, the WVTR value increases as the RH% increases due to simultaneous adsorption and desorption of water molecules in the atmosphere on the encapsulation surface [71,72]. In case of underwater conditions, the WTR test is considered the harshest environment to evaluate the water resistance because liquid water can fully cover the encapsulation surface regardless of desorption. The same as for the general WVTR, the number of liquid water molecules penetrating through a unit area of the encapsulation layers per unit of time was calculated according to the following equation [73].

$$\mathrm{WTR}\left[\mathrm{g}\,m^{-2}day^{-1}\right] = -\mathrm{n} \bullet (M_{H_2O}/M_{Ca}) \bullet \rho_{Ca} \bullet \sigma_{Ca} \bullet [\mathrm{d}(1/\mathrm{R})/\mathrm{dt}] \bullet (S_{Ca}/S_{window}). \quad (1)$$

Here, the value of n is 2, as determined by the degradation reaction of calcium to permeate water; M_{H_2O} and M_{Ca} are the molecular weights of H_2O (18 g mol^{-1}) and Ca (40 g mol^{-1}), respectively; ρ_{Ca} and σ_{Ca} are the density (1.55 g cm^{-3}) and resistivity (3.4 × 10^{-8} Ωm) of calcium, respectively; S_{Ca} is the area of the Ca (10 × 10 mm^2); and S_{window} is the transmission area of the water (10 × 10 mm^2) defined by a resin mold. The value of d(1/R)/dt was calculated according to the slope of the normalized Ca resistance plot. The WTR values of the encapsulation barrier films under direct water contact are summarized in Table 1. The WTR of the three coupled layers of Al_2O_3/Parylene C was 7.12 × 10^{-2} g m^{-2} day^{-1}, which was the best performance in the control groups. Unlike the control groups, the Ca cell with a t-SiO_2 layer exhibited almost no degradation behavior and maintained a low resistance under direct exposure to water at room temperature. Because the Ca was not oxidized sufficiently, the resistance of Ca with t-SiO_2 did not sufficiently change to allow calculating the slope for WTR. As shown in Fig. 3c, to measure the WTR of the t-SiO_2 encapsulation layer, an acceleration test was conducted by heating the slide glass substrate of the calcium sample to 85 °C on a hot plate. At 85 °C, penetration of water molecules occurs more strongly than at room temperature, which accelerates the oxidation of the calcium cell [52]. As a result of the acceleration test, the average WTR of the t-SiO_2 water barrier was 1.53 × 10^{-3} g m^{-2} day^{-1}.

Table 1
WTR of various encapsulation barriers to evaluate performance under DI water exposure.

Materials	Thickness [nm]	WTR [g m^{-2} day^{-1}]
Parylene C	500	1.94 × 10^{1} (at RT[a)])
Sputter SiO_2	500	2.48 × 10^{-1} (at RT)
PECVD SiO_2	500	2.10 × 10^{-1} (at RT)
Al_2O_3/Parylene C	50/115 × 3	7.12 × 10^{-2} (at RT)
t-SiO_2	500	1.53 × 10^{-3} (at 85 °C)

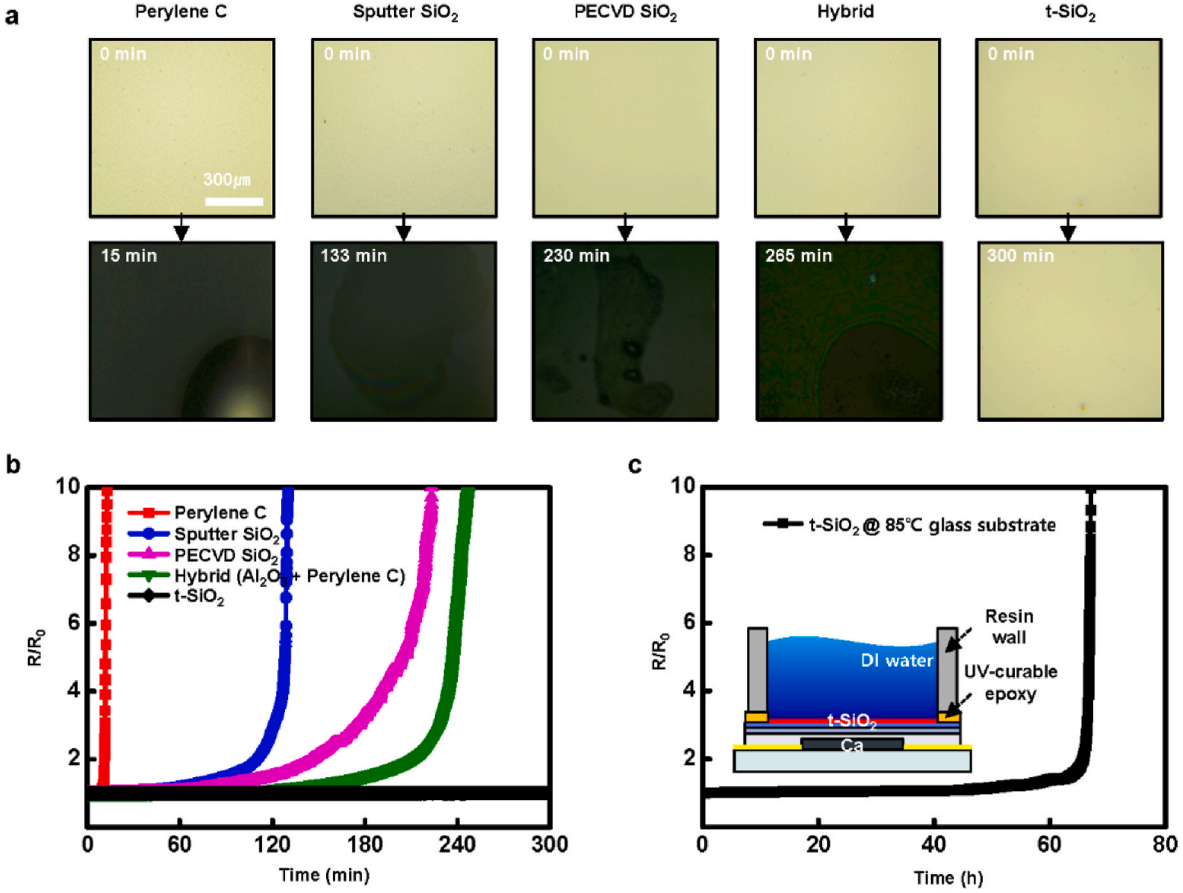

Fig. 3. Electrical calcium test for evaluation of t-SiO_2 NM moisture barrier: a) optical microscope images of calcium samples before and after electrical calcium test. b) normalized resistance vs. time curve of the calcium samples with various thin-film encapsulation materials exposed to DI water at room temperature. c) accelerated test result of calcium sample with the t-SiO_2 encapsulation layer exposed to DI water at 85 °C. [a)]Room temperature range from 22 to 25 °C.

2.4. Stability test of RT-TFE PSC

To verify the enhanced long-term stability under harsh environmental conditions of PSCs fabricated using RT-TFE, the surfaces of the encapsulated PSCs were directly exposed to DI water. First, the stabilities of the encapsulated and non-encapsulated devices exposed to DI water were compared. To confirm the degradation of the PSCs immersed in DI water, we observed the spiro-OMeTAD region, not the Au electrode region, using optical microscopy, as displayed in Fig. 4a. Before the devices were underwater they were maroon, which originated from the spiro-OMeTAD/perovskite layer [74]. After 1 min, the unencapsulated device turned bright red due to the degradation of the perovskite layer. After 1 h, the perovskite layer almost dissolved, and the device changed from maroon to blue, which originated from the spiro-OMeTAD layer (Fig. S2). After 24 h, the perovskite layer fully disappeared and the spiro-OMeTAD layer was partially delaminated in some parts. Finally, only the SnO_2 layer remained [75]. In contrast, the encapsulated PSC was not changed by water after 31 days, indicating that the encapsulated PSC did not degrade at any layer. Fig. 4b shows the J-V curves of our best-performing cell exposed to DI water at room temperature for 31 days. The t-SiO_2 moisture barrier blocked the penetration of moisture; hence, the PSC exhibited only a negligible change in performance after 31 days of exposure to water. As shown in Fig. 4c–f, the PCE changed from 17.29% to 16.94%, FF from 74.82% to 76.35%, J_{sc} from 22.27 to 21.88 mA cm^{-2}, and V_{oc} from 1.04 to 1.01 V after 31 days. Moreover, the RT-TFE device maintained 98.98% of its initial efficiency after 31 days of exposure to DI water at room temperature. The performance was maintained at the same level as that of the RT-TFE PSCs exposed to an ambient environment (25 °C, RH 50%) over 31 days (Fig. S3). This was the longest-surviving TFE PSC reported to date, in terms of exhibiting excellent long-term stability in an underwater environment (Table S1). Furthermore, this superior t-SiO_2 barrier directly blocked water molecules and exhibited great potential for applications in PSCs for outdoor use and floating solar panels.

3. Conclusion

In summary, we report on RT-TFE PSCs for enhancing long-term protection against the penetration of water molecules by encapsulating photovoltaic cells with 500-nm-thick t-SiO_2 NM at room

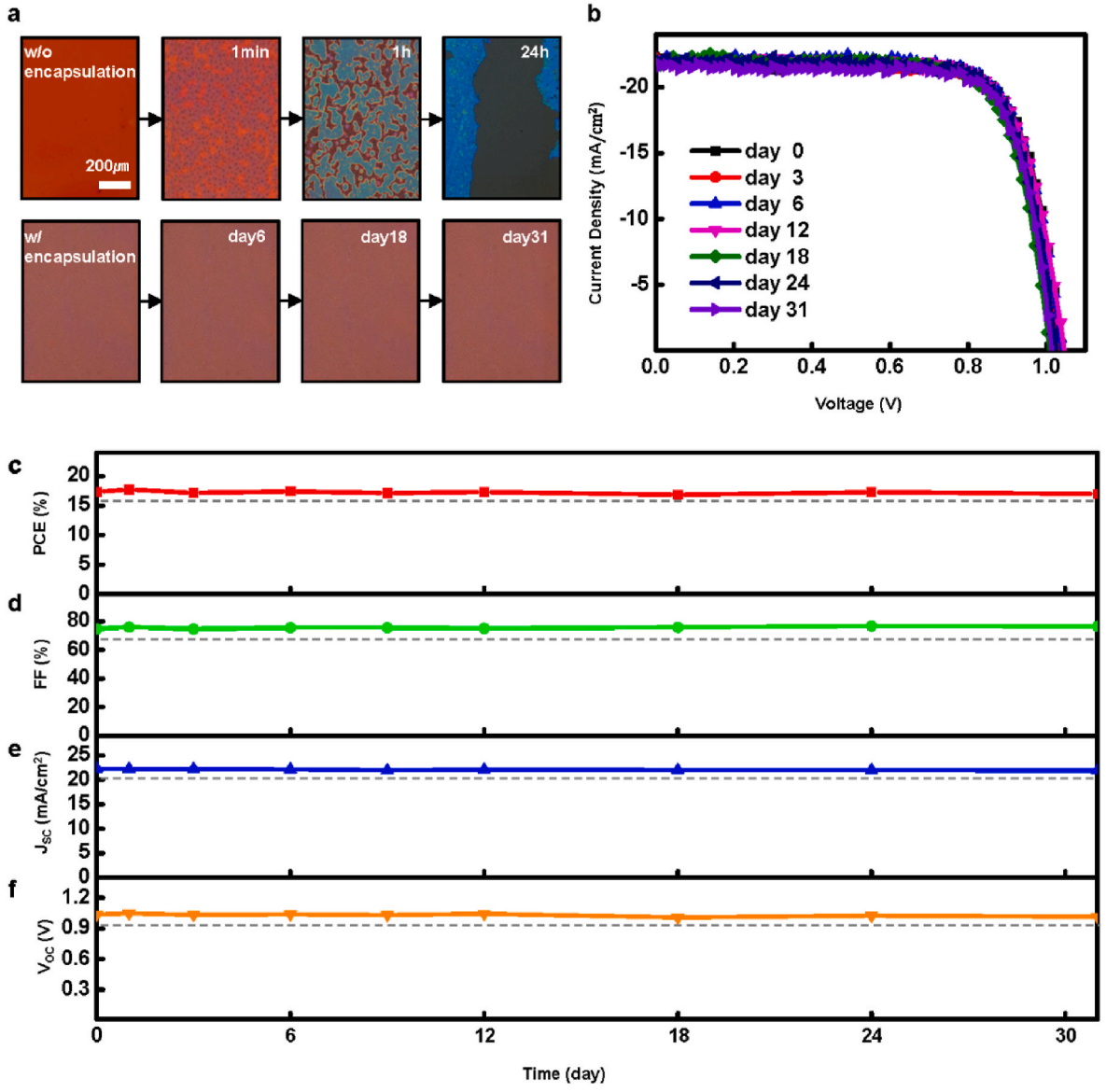

Fig. 4. Stability of RT-TFE PSC exposed to underwater condition at room temperature: a) optical microscope image of pristine PSC and RT-TFE PSC exposed under water over time; b) J-V curves of submerged RT-RFE PSC from days 0–31; c–f) device parameters of RT-TFE PSC during the stability test: c) PCE, d) FF, e) Jsc, f)Voc.

temperature to minimize the performance degradation of devices. The defect-free SiO_2 NM was grown on a handling wafer through thermal oxidation at 1100 °C and was sequentially stacked with a buffer layer and an adhesive layer. By transferring the prepared encapsulation layer to the PSC in an inert environment and removing the handling wafer through an XeF_2 etcher, all processes could be performed at room temperature. After encapsulation, the RT-TFE PSCs only displayed an average PCE decrease of 0.012% compared to their initial state. When t-SiO_2 was integrated with the device, it exhibited excellent WTR, approximately 1×10^{-3} g m^{-2} day^{-1}, and water molecule blocking properties under the 85 °C acceleration condition. Furthermore, the outermost layer of RT-TFE PSC, t-SiO_2 NM, successfully protected the device from water molecules at room temperature for 31 days and maintained more than 98% of its initial PCE. Our research suggests that the RT-TFE strategy is the first demonstration of a damage-less encapsulation process for PSCs with an inorganic nanomembrane moisture barrier grown under a high temperature. Furthermore, our encapsulation method of transferring thermally grown oxide on a solar cell suggests the possibility of achieving scale-up by transferring it to multiple cells. This would provide a new commercialization route to prolong the lifetime of large-area PSCs by protecting the devices from rain and snow which are common in outdoor environments as well as humid conditions, rendering them suitable for applications in aquatic environments such as floating solar panels in the near future.

4. Experimental section

4.1. Materials

All the materials were purchased from commercial companies. The SnO_2 colloid precursor (tin (IV) oxide, 15% in H_2O colloidal dispersion) was purchased from Alfa Aesar. The PbI_2 was purchased from TCI. Bis (trifluoromethylsulfonyl)imide lithium salt (Li-TFSI) and the anhydrous solvents were purchased from Sigma-Aldrich. Methylammonium iodide (MAI) was purchased from GreatCell Solar. 2,2′,7,7′-tetrakis (N,N-dip-methoxyphenylamine)-9,9′-spirobifluorene (Spiro-OMeTAD) was purchased from LumTech. SU-8 2010 was purchased from Microchem. Kwik-Sil was purchased from World Precision Instruments. Finally, polydimethylsiloxane (PDMS, Sylgard 187) was purchased as a two-component kit containing base and curing agent from Dow Corning.

4.2. Perovskite solar cells (PSCs) fabrication and characterization

The patterned fluorine-doped thin oxide (FTO) glass was sequentially cleaned by ultra-sonication for 15 min in detergent, deionized (DI) water, acetone, and isopropyl alcohol (IPA). The cleaned FTO glass was then treated with UV/ozone for 30 min. An electron transport layer (ETL) was deposited by spin-coating SnO_2 solution (diluted with DI water to 2.75%) on the prepared substrate at 3000 rpm for 30 s, annealed at 150 °C for 30 min, then UV/ozone treated for 20 min.

To prepare the $MAPbI_3$ perovskite precursor solution of 1.2 M, a mixed powder consisting of MAI (190.8 mg) and PbI_2 (553.2 mg) was dissolved in 1 mL mixed solvent of dimethylformamide (DMF) and dimethyl sulfoxide (DMSO) (volume ratio of 4:1). The precursor solution was then spin-coated onto the substrate at 1000 rpm for 5 s and 5000 rpm for 50 s. In the second step, 800 μL of chlorobenzene was smoothly dropped onto the film at 45 s remains in the 5000 rpm spinning process. After deposition, the film was directly annealed at 100 °C for 15 min in an N_2-filled glove box.

The spiro-OMeTAD solution was prepared by dissolving 91 mg spiro-OMeTAD in 1 mL chlorobenzene after adding 20.9 μL of Li-TFSI in acetonitrile (517 mg/mL) and 35.4 μL of 4-tert-Butylpyridine (t-BP). The prepared solution was then spin-coated on the perovskite layer at 3500 rpm for 40 s. As a counter electrode, 100 nm of Au was deposited by thermal evaporation through a shadow mask under high vacuum conditions (under 10^{-5} Torr).

4.3. Room temperature thin-film encapsulation(RT-TFE) process

Preparation of the encapsulation layer for RT-TFE began with a thermally grown 500 nm SiO_2 (t-SiO_2) layer fabricated by wet oxidation (in O_2/H_2O) at 1100 °C performed on a standard silicon wafer (675 μm thickness, 6 inch diameter, SILTRON). Through a mechanical grinding process, the thickness of the wet-oxidized wafer was then reduced to less than 100 μm (5 μm thickness deviation, back side polished like a mirror, Freemteck). Reactive ion etching (RIE, Young Vacuum System) with O_2 plasma activated the SiO_2 surface. Subsequently, spin coating, soft baking, UV irradiation, and hard baking of the negative photoresist SU-8 2010 with a thickness of 10 μm were performed. After activating the surface of the SU-8-like SiO_2 using RIE, spin-coating Kwik-Sil with a thickness of 14 μm was conducted in a glove box filled with N_2 gas. Then, the PSC and the prepared encapsulation layer were immediately bonded by applying a pressure of approximately 50 kPa using a metal jig (Kistech) and cured at room temperature. A 100 μm thick bulk wafer was removed using a XeF_2 Si release etcher (SPTS Technologies) with XeF_2 gas, leaving an encapsulation layer.

4.4. Photovoltaic performance measurement

The current density-voltage (J-V) curves of the PSCs were measured using a Keithley 2602A Source Meter under simulated AM 1.5G illumination (100 $mWcm^{-2}$) with a solar simulator (K3000 model, McScience) calibrated by a standard Si reference cell (K801S–K067, McScience). The active area of the devices was defined as 0.0875 cm^2 using a square patterned mask during the measurements. The external quantum efficiency (EQE) spectrum was measured using an incident photon-to-current conversion efficiency (IPCE) consisting of a Xenon lamp (Newport, 450 W) as a light source and a monochromator.

4.5. Electrical calcium test

The patterned aluminum (Al) and calcium (Ca) electrodes were deposited on the glass substrate at 150 and 300 nm, respectively. The patterned Ca area was measured as 1×1 cm^2. The encapsulation process was conducted in a glove box using RT-TFE. Each encapsulation layer was deposited on a single crystal silicon wafer (100 μm thickness, 1.5×1.5 cm^2 area). The parylene C encapsulation layer (500 nm thickness) was prepared by using a parylene coater (LAVIDA, Femto Science) at a deposition temperature of 230 °C. Each SiO_2 encapsulation layer (500 nm thickness) was prepared by using a sputter (KVS-T8860, Korea Vacuum), plasma-enhanced chemical vapor deposition (PECVD) (URECA 2000, Jusung Engineering) with deposition frequency 13.56 MHz and temperature of 180 °C. Furthermore, an Al_2O_3/Parylene C (50/115 nm thickness) encapsulation layer was prepared using atomic layer deposition (ALD) (Large-area ALD system, I Tech U) with a deposition temperature of 150 °C and a parylene coater (LAVIDA, Femto Science) with a deposition temperature of 230 °C, which was repeated three times. The encapsulated Ca cells were attached using a resin mold filled with 1.5 ml of DI water. The active area exposed to water was measured as 1 cm^2. The electrical resistance (R) of the Ca was measured using a multimeter (Agilent) in underwater conditions at 25 and 85 °C, respectively.

4.6. Stability test

For the direct water contact resistance test, a resin mold filled with 1.5 ml DI water was covered on the unencapsulated/encapsulated perovskite solar cell in an N_2-filled condition. The unencapsulated/encapsulated perovskite solar cells were then attached to the mold, which was filled with 1.5 ml of DI water. The active area exposed to water was measured as 0.6 cm^2 and the stability test was conducted under dry conditions at room temperature.

CRediT authorship contribution statement

Myeongki Cho: Conceptualization, Methodology, Formal analysis, Investigation, Writing – original draft, Visualization, contributed equally to this work. **Gyeong G. Jeon:** Conceptualization, Methodology, Formal analysis, Investigation, Writing – original draft, and, Visualization, contributed equally to this work. **Mingyu Sang:** Conceptualization, Methodology, Formal analysis, Investigation, Writing – original draft, Visualization, contributed equally to this work. **Tae Soo Kim:** Formal analysis, Investigation. **Jungmin Suh:** Formal analysis, Investigation. **So Jeong Shin:** Investigation. **Min Jun Choi:** Investigation. **Hyun Woo Kim:** Investigation. **Kyubeen Kim:** Investigation. **Ju Young Lee:** Investigation. **Jeong Yeon Noh:** Investigation. **Jong H. Kim:** Resources, Writing – review & editing. **Jincheol Kim:** Conceptualization, Methodology, Writing – review & editing, Supervision. **Nochang Park:** Conceptualization, Methodology, Resources, Writing – review & editing, Supervision, Funding acquisition. **Ki Jun Yu:** Conceptualization, Methodology, Resources, Writing – review & editing, Supervision, Project administration, Funding acquisition.

Declaration of competing interest

The authors declare that they have no known competing financial interests or personal relationships that could have appeared to influence the work reported in this paper.

Data availability

Data will be made available on request.

Acknowledgements

This work acknowledges the support received from the National Research Foundation of Korea (Grant Nos. NRF-2019R1A2C2086085, NRF-2021R1A4A1031437, NRF-2021K1A4A7A03093854, and NRF-2022M3I8A2085439) and the KIST Institutional Program (Project No. 2E31603-22-140). J.K. acknowledges the support of the Australian Renewable Energy Agency (Project 2020/RND003).

Appendix A. Supplementary data

Supplementary data to this article can be found online at https://doi.org/10.1016/j.jpowsour.2023.232810.

References

[1] W.S. Yang, J.H. Noh, N.J. Jeon, Y.C. Kim, S. Ryu, J. Seo, S.I. Seok, Science 348 (2015) 1234–1237.
[2] S.-H. Turren-Cruz, M. Saliba, M.T. Mayer, H. Juárez-Santiesteban, X. Mathew, L. Nienhaus, W. Tress, M.P. Erodici, M.-J. Sher, M.G. Bawendi, Energy Environ. Sci. 11 (2018) 78–86.
[3] A.A. Zhumekenov, M.I. Saidaminov, M.A. Haque, E. Alarousu, S.P. Sarmah, B. Murali, I. Dursun, X.-H. Miao, A.L. Abdelhady, T. Wu, ACS Energy Lett. 1 (2016) 32–37.
[4] A. Miyata, A. Mitioglu, P. Plochocka, O. Portugall, J.T.-W. Wang, S.D. Stranks, H. J. Snaith, R.J. Nicholas, Nat. Phys. 11 (2015) 582–587.
[5] G.E. Eperon, S.D. Stranks, C. Menelaou, M.B. Johnston, L.M. Herz, H.J. Snaith, Energy Environ. Sci. 7 (2014) 982–988.
[6] C. Roldán-Carmona, O. Malinkiewicz, A. Soriano, G.M. Espallargas, A. Garcia, P. Reinecke, T. Kroyer, M.I. Dar, M.K. Nazeeruddin, H.J. Bolink, Energy Environ. Sci. 7 (2014) 994–997.
[7] M. Kaltenbrunner, G. Adam, E.D. Głowacki, M. Drack, R. Schwödiauer, L. Leonat, D.H. Apaydin, H. Groiss, M.C. Scharber, M.S. White, Nat. Mater. 14 (2015) 1032–1039.
[8] A.T. Barrows, A.J. Pearson, C.K. Kwak, A.D. Dunbar, A.R. Buckley, D.G. Lidzey, Energy Environ. Sci. 7 (2014) 2944–2950.
[9] K. Hwang, Y.S. Jung, Y.J. Heo, F.H. Scholes, S.E. Watkins, J. Subbiah, D.J. Jones, D.Y. Kim, D. Vak, Adv. Mater. 27 (2015) 1241–1247.
[10] P. Li, C. Liang, B. Bao, Y. Li, X. Hu, Y. Wang, Y. Zhang, F. Li, G. Shao, Y. Song, Nano Energy 46 (2018) 203–211.
[11] X. Li, D. Bi, C. Yi, J.-D. Décoppet, J. Luo, S.M. Zakeeruddin, A. Hagfeldt, M. Grätzel, Science 353 (2016) 58–62.
[12] A. Kojima, K. Teshima, Y. Shirai, T. Miyasaka, J. Am. Chem. Soc. 131 (2009) 6050–6051.
[13] M.A. Green, E.D. Dunlop, J. Hohl-Ebinger, M. Yoshita, N. Kopidakis, X. Hao, Prog. Photovoltaics Res. Appl. (2021) 29.
[14] R. Wang, M. Mujahid, Y. Duan, Z.K. Wang, J. Xue, Y. Yang, Adv. Funct. Mater. 29 (2019), 1808843.
[15] C.C. Boyd, R. Cheacharoen, T. Leijtens, M.D. McGehee, Chem. Rev. 119 (2018) 3418–3451.
[16] S. Zhang, Z. Liu, W. Zhang, Z. Jiang, W. Chen, R. Chen, Y. Huang, Z. Yang, Y. Zhang, L. Han, Adv. Energy Mater. 10 (2020), 2001610.
[17] J. Yang, B.D. Siempelkamp, D. Liu, T.L. Kelly, ACS Nano 9 (2015) 1955–1963.
[18] J.M. Frost, K.T. Butler, F. Brivio, C.H. Hendon, M. Van Schilfgaarde, A. Walsh, Nano Lett. 14 (2014) 2584–2590.
[19] J. Huang, S. Tan, P.D. Lund, H. Zhou, Energy Environ. Sci. 10 (2017) 2284–2311.
[20] M.K. Rao, D. Sangeetha, M. Selvakumar, Y. Sudhakar, M. Mahesha, Sol. Energy 218 (2021) 469–491.
[21] F.J. Ramos, T. Maindron, S. Béchu, A. Rebai, M. Frégnaux, M. Bouttemy, J. Rousset, P. Schulz, N. Schneider, Sustain. Energy Fuels 2 (2018) 2468–2479.
[22] Y.I. Lee, N.J. Jeon, B.J. Kim, H. Shim, T.Y. Yang, S.I. Seok, J. Seo, S.G. Im, Adv. Energy Mater. 8 (2018), 1701928.
[23] L. Shi, T.L. Young, J. Kim, Y. Sheng, L. Wang, Y. Chen, Z. Feng, M.J. Keevers, X. Hao, P.J. Verlinden, ACS Appl. Mater. Interfaces 9 (2017) 25073–25081.
[24] F. Matteocci, L. Cinà, E. Lamanna, S. Cacovich, G. Divitini, P.A. Midgley, C. Ducati, A. Di Carlo, Nano Energy 30 (2016) 162–172.
[25] Q. Dong, F. Liu, M.K. Wong, H.W. Tam, A.B. Djurišić, A. Ng, C. Surya, W.K. Chan, A.M.C. Ng, ChemSusChem 9 (2016) 2597–2603.
[26] E. Ramasamy, V. Karthikeyan, K. Rameshkumar, G. Veerappan, Mater. Lett. 250 (2019) 51–54.
[27] J. Martins, S. Emami, R. Madureira, J. Mendes, D. Ivanou, A. Mendes, J. Mater. Chem. 8 (2020) 20037–20046.
[28] J. Zhao, K. Brinkmann, T. Hu, N. Pourdavoud, T. Becker, T. Gahlmann, R. Heiderhoff, A. Polywka, P. Görrn, Y. Chen, Adv. Energy Mater. 7 (2017), 1602599.
[29] H. Wang, Y. Zhao, Z. Wang, Y. Liu, Z. Zhao, G. Xu, T.-H. Han, J.-W. Lee, C. Chen, D. Bao, Nano Energy 69 (2020), 104375.
[30] O. Zhao, Y. Ding, Z. Pan, N. Rolston, J. Zhang, R.H. Dauskardt, ACS Appl. Mater. Interfaces 12 (2020) 26405–26412.
[31] A. Babayigit, A. Ethirajan, M. Muller, B. Conings, Nat. Mater. 15 (2016) 247–251.
[32] J. Kim, D. Seong, H. Kwon, S. Jin, H. Kim, Y. Kim, Y. Jeong, K. Lee, S.J. Kwon, M. Shin, ACS Nano 15 (2021) 20127–20135.
[33] L.J. Sutherland, H.C. Weerasinghe, G.P. Simon, Adv. Energy Mater. 11 (2021), 2101383.
[34] S. Castro-Hermosa, M. Top, J. Dagar, J. Fahlteich, T.M. Brown, Adv. Electronic. Mater. 5 (2019), 1800978.
[35] S.S. Shin, E.J. Yeom, W.S. Yang, S. Hur, M.G. Kim, J. Im, J. Seo, J.H. Noh, S.I. Seok, Science 356 (2017) 167–171.
[36] T. Leijtens, G.E. Eperon, S. Pathak, A. Abate, M.M. Lee, H.J. Snaith, Nat. Commun. 4 (2013) 1–8.
[37] B. Conings, J. Drijkoningen, N. Gauquelin, A. Babayigit, J. D'Haen, L. D'Olieslaeger, A. Ethirajan, J. Verbeeck, J. Manca, E. Mosconi, Adv. Energy Mater. 5 (2015), 1500477.
[38] R. Paetzold, A. Winnacker, D. Henseler, V. Cesari, K. Heuser, Rev. Sci. Instrum. 74 (2003) 5147–5150.
[39] R. Cheacharoen, N. Rolston, D. Harwood, K.A. Bush, R.H. Dauskardt, M. D. McGehee, Energy Environ. Sci. 11 (2018) 144–150.
[40] L. Shi, M.P. Bucknall, T.L. Young, M. Zhang, L. Hu, J. Bing, D.S. Lee, J. Kim, T. Wu, N. Takamure, Science 368 (2020), eaba2412.
[41] Z. Fu, M. Xu, Y. Sheng, Z. Yan, J. Meng, C. Tong, D. Li, Z. Wan, Y. Ming, A. Mei, Adv. Funct. Mater. 29 (2019), 1809129.
[42] P.F. Carcia, R. McLean, M. Reilly, M. Groner, S. George, Appl. Phys. Lett. 89 (2006), 031915.
[43] S. Sarkar, J.H. Culp, J.T. Whyland, M. Garvan, V. Misra, Org. Electron. 11 (2010) 1896–1900.
[44] R. Singh, S. Ghosh, A.S. Subbiah, N. Mahuli, S.K. Sarkar, Sol. Energy Mater. Sol. Cell. 205 (2020), 110289.
[45] J. Meyer, a.D. Schneidenbach, T. Winkler, S. Hamwi, T. Weimann, P. Hinze, S. Ammermann, H.-H. Johannes, T. Riedl, a. Kowalsky, Appl. Phys. Lett. 94 (2009) 157.
[46] T. Chen, D. Wuu, C. Wu, C. Chiang, Y. Chen, R.-H. Horng, J. Electrochem. Soc. 153 (2006) F244.
[47] S.-W. Seo, H. Chae, S. Joon Seo, H. Kyoon Chung, S. Min Cho, Appl. Phys. Lett. 102 (2013), 161908.
[48] S. Seo, S. Jeong, C. Bae, N.G. Park, H. Shin, Adv. Mater. 30 (2018), 1801010.
[49] J. Jin, H. Li, W. Bi, C. Chen, B. Zhang, L. Xu, B. Dong, H. Song, Q. Dai, Sol. Energy 198 (2020) 187–193.
[50] D. Yu, Y.-Q. Yang, Z. Chen, Y. Tao, Y.-F. Liu, Opt Commun. 362 (2016) 43–49.
[51] Q. Lu, Z. Yang, X. Meng, Y. Yue, M.A. Ahmad, W. Zhang, S. Zhang, Y. Zhang, Z. Liu, W. Chen, Adv. Funct. Mater. 31 (2021), 2100151.
[52] H. Fang, J. Zhao, K.J. Yu, E. Song, A.B. Farimani, C.-H. Chiang, X. Jin, Y. Xue, D. Xu, W. Du, Proc. Natl. Acad. Sci. USA 113 (2016) 11682–11687.
[53] S. Lee, J.-H. Han, S.-H. Lee, G.-H. Baek, J.-S. Park, JOM (J. Occup. Med.) 71 (2019) 197–211.
[54] J. Wu, F. Fei, C. Wei, X. Chen, S. Nie, D. Zhang, W. Su, Z. Cui, RSC Adv. 8 (2018) 5721–5727.
[55] W. Xiao, D. Yu, S.F. Bo, Y.Y. Qiang, Y. Dan, C. Ping, D.Y. Hui, Z. Yi, RSC Adv. 4 (2014) 43850–43856.

[56] Y. Lv, H. Zhang, R. Liu, Y. Sun, W. Huang, ACS Appl. Mater. Interfaces 12 (2020) 27277–27285.
[57] Y.K. Lee, K.J. Yu, Y. Kim, Y. Yoon, Z. Xie, E. Song, H. Luan, X. Feng, Y. Huang, J. A. Rogers, ACS Appl. Mater. Interfaces 9 (2017) 42633–42638.
[58] H. Fang, K.J. Yu, C. Gloschat, Z. Yang, E. Song, C.-H. Chiang, J. Zhao, S.M. Won, S. Xu, M. Trumpis, Nat. Biomed. Eng. 1 (2017) 1–12.
[59] L. Li, Y. Chen, Z. Liu, Q. Chen, X. Wang, H. Zhou, Adv. Mater. 28 (2016) 9862–9868.
[60] T. Malinauskas, D. Tomkute-Luksiene, R.d. Sens, M. Daskeviciene, R. Send, H. Wonneberger, V. Jankauskas, I. Bruder, V. Getautis, ACS Appl. Mater. Interfaces 7 (2015) 11107–11116.
[61] J. Kim, N. Park, J.S. Yun, S. Huang, M.A. Green, A.W. Ho-Baillie, Sol. Energy Mater. Sol. Cell. 162 (2017) 41–46.
[62] X. Zhao, H.-S. Kim, J.-Y. Seo, N.-G. Park, ACS Appl. Mater. Interfaces 9 (2017) 7148–7153.
[63] K.-P. Yoo, N.-K. Min, Thin Solid Films 516 (2008) 3586–3589.
[64] M. Jeong, I.W. Choi, E.M. Go, Y. Cho, M. Kim, B. Lee, S. Jeong, Y. Jo, H.W. Choi, J. Lee, Science 369 (2020) 1615–1620.
[65] Z. Yang, J. Dou, S. Kou, J. Dang, Y. Ji, G. Yang, W.Q. Wu, D.B. Kuang, M. Wang, Adv. Funct. Mater. 30 (2020), 1910710.
[66] G. Tumen-Ulzii, C. Qin, T. Matsushima, M.R. Leyden, U. Balijipalli, D. Klotz, C. Adachi, Solar RRL 4 (2020), 2000305.
[67] C.D. Bailie, E.L. Unger, S.M. Zakeeruddin, M. Grätzel, M.D. McGehee, Phys. Chem. Chem. Phys. 16 (2014) 4864–4870.
[68] K. Domanski, E.A. Alharbi, A. Hagfeldt, M. Grätzel, W. Tress, Nat. Energy 3 (2018) 61–67.
[69] B. Xu, J. Huang, H. Ågren, L. Kloo, A. Hagfeldt, L. Sun, ChemSusChem 7 (2014) 3252–3256.
[70] Y. Zhang, A. Kirs, F. Ambroz, C.T. Lin, A.S. Bati, I.P. Parkin, J.G. Shapter, M. Batmunkh, T.J. Macdonald, Small Methods 5 (2021), 2000744.
[71] J. Bertrand, D. Higgs, M. Young, S. George, J. Phys. Chem. 117 (2013) 12026–12034.
[72] O. Sneh, M.A. Cameron, S.M. George, Surf. Sci. 364 (1996) 61–78.
[73] L.H. Kim, Y.J. Jeong, T.K. An, S. Park, J.H. Jang, S. Nam, J. Jang, S.H. Kim, C. E. Park, Phys. Chem. Chem. Phys. 18 (2016) 1042–1049.
[74] H. Kim, J. Lee, B. Kim, H.R. Byun, S.H. Kim, H.M. Oh, S. Baik, M.S. Jeong, Sci. Rep. 9 (2019) 1–6.
[75] S. Ma, S. Pang, H. Dong, X. Xie, G. Liu, P. Dong, D. Liu, W. Zhu, H. Xi, D. Chen, Polymers 14 (2022) 343.